Journal of Earth Sciences and Geotechnical Engineering, vol. 6, no.2, 2016, 101-114
ISSN: 1792-9040 (print), 1792-9660 (online)
Scienpress Ltd, 2016

GPR Q* Determination from CMP Data as a Means of measuring Frequency Dependent Attenuation

Aisha A. Kana[1]

Abstract

Attenuation and velocity in the ground are the major controls on the propagation of GPR signals in the ground and depend on electrical conductivity and dielectric permeability. In addition to these, attenuation of radar signals is frequency dependent; it increases with increase in frequency. The attraction of the GPR method lies in its short wavelength and hence good resolution, i.e. because of the high frequency used; but unfortunately, this makes it prone to attenuation thus limiting depth of penetration of the radar waves. It is therefore necessary that this dependence on frequency be understood, better still, site specific characterization is important. The attenuation coefficient (α, m^{-1}), can be estimated using site specific laboratory or field estimates of electrical conductivity; this may not always be practicable, and hence further means of characterizing attenuation is required.

This paper reports on frequency dependent attenuation characterization using the spectral ratios method. The method involves comparing spectra of reflection from successive intervals generated from a CMP section to estimate the GPR quality factor Q* and from there, attenuation. The analysis was applied to two CMP data sets acquired in a limestone quarry, along the quarry floor using 500MHz antennas. The analysis showed that attenuation increases with increase in frequency from $0.2m^{-1}$ at 200MHz up to $1.2\ m^{-1}$ at 800MHz. The analysis serves to improve *in – situ* characterization of attenuation especially where it is required for further analysis e.g. amplitude variation with offset analysis of GPR data.

Keywords: GPR, Q*, attenuation, CMP

1 Introduction

Attenuation and velocity in the ground are the major controls on the propagation of radar waves; these in turn depend on the electrical properties, mainly electrical conductivity and dielectric permittivity. Attenuation of radar waves is frequency dependent, owing to water relaxation mechanisms and ionic conductivity of pore solution if present, which creates frequency dependence at low frequencies. The attraction of the GPR method lies in its

[1]Department of Geology and Mining, Nasarawa State University, Keffi, Nigeria.

short wavelength and hence good resolution, i.e. because of the high frequency used; but unfortunately, this makes it prone to attenuation thus limiting depth of penetration of the radar waves. The attenuation coefficient (α, m^{-1}), can be estimated using site specific laboratory or field estimates of electrical conductivity, e.g. in [11] and [5]. This may not always be practicable, and hence further means of characterizing attenuation has been proposed, especially in geological media, which involves synthetic data analysis and comparison with field data.
In the following analysis, α was characterised in a quarry, Threshfield quarry in Yorkshire United Kingdom, extracting Carboniferous Limestone. Frequency dependence of attenuation was measured from GPR Q*, determined through spectral ratios analysis on CMP data acquired on the quarry floor.

2 Spectral Ratios Analysis - Theory

In GPR applications, a common assumption is that attenuation, within the signal bandwidth (an octave either side of the centre frequency) is linear with frequency. The general form of a propagating GPR wave is given by equation 1.

$$A = A_0 exp^{(-\alpha r)} exp^{(iw(t-r/c))} \quad (1)$$

Where A is amplitude; t is time; r is distance or ray path; c is phase velocity; A_0 is amplitude at $r = 0$, $t = 0$; α is attenuation coefficient; ω is angular frequency and $i = \sqrt{-1}$.
The properties c, α and therefore A are frequency dependent. In seismic analysis, this frequency dependent wave propagation has been described by Q, the seismic quality factor and the phase velocity [1]. Seismic Q is defined in Sherriff, (2002) as the ratio of 2π times the peak energy to the energy dissipated in one cycle (equation 2). Closely related to the seismic Q is [11] Q^*, the GPR attenuation quality factor. In their paper, they showed that GPR attenuation can be approximated by a linear function of frequency over the frequency bandwidth of GPR instruments. Q^* in their paper is defined as the slope of the straight line portion of an attenuation versus frequency graph within the signal bandwidth (equation 3). They assumed that Q^* within the signal bandwidth is constant and therefore α is, within this bandwidth, linear with frequency. They introduced equation 4 so that α_0 represents all effects outside the frequency bandwidth of the signal.

$$Q = \frac{\omega}{2c\alpha} \quad (2)$$

$$Q^* = \frac{1}{2c}\frac{\Delta\omega}{\Delta\alpha} \quad (3)$$

$$\alpha = \alpha_0 + \frac{\omega}{2cQ^*} \quad (4)$$

Q^* value calculated within the signal bandwidth describes adequately attenuation in most rocks [4], thus it is necessary to find a means of extracting it from GPR data. The spectral ratios method described below is an approach for doing this.
Spectral ratio analysis involves calculating the spectra of a pair of wavelets e.g. reflections from the two surfaces bounding an interval, to obtain amplitude decay versus frequency plot and, from there the slope of the straight line portion within the signal bandwidth. Combining equations 2 and 4 gives:

$$\frac{A}{A_0} = R.G.exp^{\left(-\alpha_0 r - \frac{\omega r}{2cQ*}\right)} \quad (5)$$

That is, considering only the wave amplitude; *R* and *G* are frequency independent reflection/transmission and geometric spreading respectively. Replacing *c* in equation 5 by r/t, and ω by $2\pi f$ gives:

$$\frac{A}{A_0} = \left[R.G.exp^{(-\alpha_0 r)}\right]\left[exp^{\left(-\frac{\pi f t}{Q*}\right)}\right] \quad (6)$$

Taking the natural log of both sides of equation 8 gives:

$$ln\left[\frac{A}{A_0}\right] = [ln(R.G) - \alpha_r r] - \frac{\pi t}{Q*}.f \quad (7)$$

Plotting $ln\left[\frac{A}{A_0}\right]$ versus f gives a linear trend with slope = $-\frac{\pi t}{Q*}$, where *t* is the travel time difference between the two wavelets; *R*, *G*, and α_0 are discarded in the intercept term that isn't used in estimating *Q**. The slope obtained in this manner is used to calculate *Q** and subsequently attenuation in the interval of interest using equation 3. The theoretical basis and the method itself is explained in detail in: [7], [9] and [3]; all applied to seismic data. Extracting *Q* from CMP data was discussed in [3] where a plot of $-\frac{\pi t}{Q*}$ versus derived offset – by offset for a single reflection relative to a reference source wavelet, was extrapolated to give a zero offset spectral ratio slope and hence a source to reflector Q value pairs which are subsequently used to characterize attenuation in a layer. More recently, in [2], a refinement of this after [6] was applied to GPR data, and the spectral ratios of common emergence angle pairs are compared to eliminate the need for antennae pattern corrections.

In this analysis, I use the same approach outlined in [2], to characterize attenuation in the field site. To extract a *Q** value for an interval in a CMP section, two wavelets travelling with the same ray path geometry in the overburden but one reflected from the top and one from the bottom surfaces of the interval of interest i.e. from sequential reflections need to be compared. This is done by simple 1D ray tracing after the basic processing steps have been applied to the data and a velocity – depth model is available. After selecting pairs of wavelets with the same emergence angles, a segment of data containing the wavelet needs to be selected, a process which depends on the centre frequency and hence period of the GPR pulse.

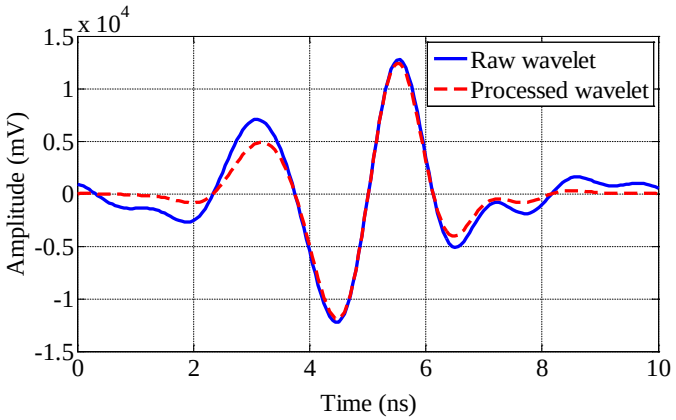

Figure 1: Wavelet analysis: a plot of raw and processed (after de – trending and applying a Hann taper) w_1 wavelet.

This was achieved through visual examination of the traces, bearing in mind the dominant period of the GPR signal (2ns for the wavelet in figure 1), thus selecting a window long enough to enclose the wavelet, but short enough to avoid including other events. The wavelets are tapered with a Hann window function which tapers either side of the wavelet to reduce spectral leakage during the fast Fourier transform (fft) of the wavelet; they are then de - trended to centre the wavelet about zero amplitude, and remove frequencies below the lowest harmonic. Figure 1 shows a wavelet before and after tapering and de - trending.

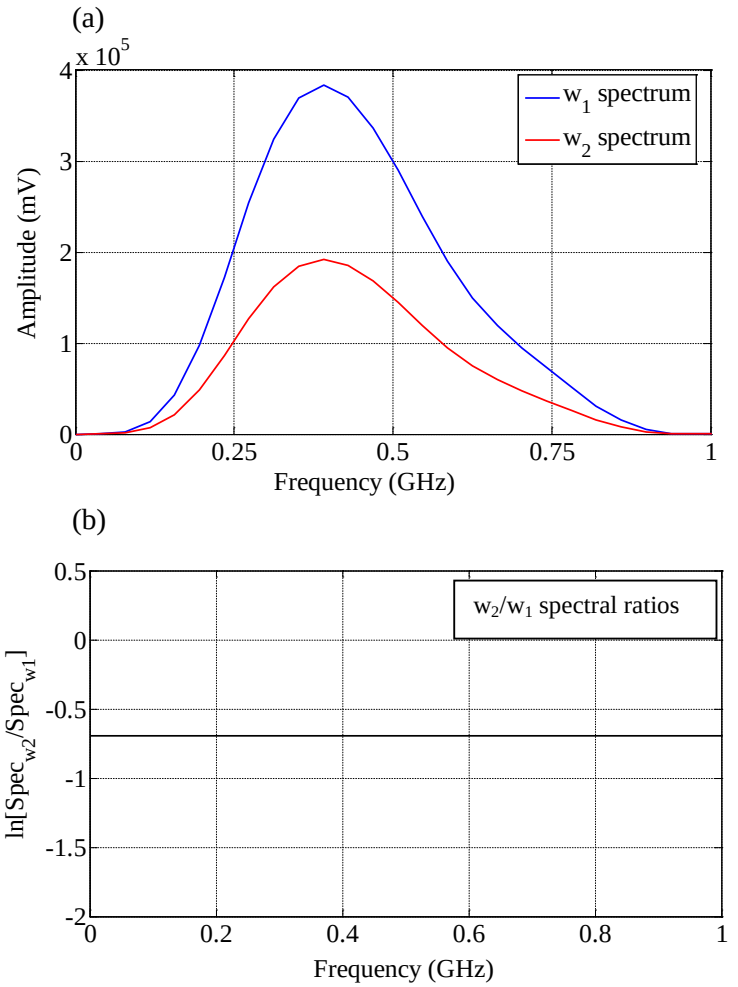

Figure 2: Spectral ratios analysis for the wavelet in figure 3; (a) plots the spectra for the wavelet and a scaled version of the wavelet, (b) plots the spectral ratios between the wavelet and its scaled (by 0.7) version.

The spectra of the wavelets are then taken using the fft; and the ratio: $ln\left[\frac{A}{A_0}\right]$ is then plotted against frequency (f). The slope of the linear portion within the signal bandwidth is then taken which is proportional to 1/Q* (equation 7), and then, α is obtained using equation 8 below (equation 17 in [11].

$$\alpha = \frac{\omega}{2vQ*}. \tag{8}$$

Where $\omega = 2\pi f$, v is velocity in the interval being analysed.
This processing flow was coded in MATLAB®; to test and validate the code, I calculated the spectral ratios between a wavelet recorded with 500MHz GPR antennae facing each other, and its scaled version. For convenience, I will call the wavelet w_1 and the scaled wavelet w_2. This simulates a layer with infinite Q; w_1 and w_2 will be identical except in their absolute amplitudes due to more geometric spreading affecting w_2 relative to w_1 and

therefore, the spectral ratio plot for these two wavelets will be flat. I scaled w_2 by a factor of 0.7; their spectra and corresponding spectral ratios are shown in figures 2a and 2b respectively. In figure 2b, the spectral ratio graph is flat meaning the code is working as it should.

CMP data:

In applying the spectral ratios approach to CMP data, GPR traces containing reflections from the top and bottom surfaces defining an interval, and recorded at a single particular offset, *cannot* be used to measure the GPR *Q**. It therefore becomes mandatory to extract, from the CMP data, wavelet pairs defining an interval of interest, which have the same take off and emergence angles; hence (except at zero – offset) not recorded at the same offset. For a single trace recorded at a non – zero offset using the CMP survey geometry, each successive wavelet reflected has a different ray path and therefore a different radiation angle i.e. emergence angle for each reflection is different (figure 3). The emergence angle for a ray incident on a horizontal and planar surface is the angle measured from the normal to the surface. The emergence angle can be computed iteratively by 1D ray tracing according to Snell's law assuming horizontal layers with constant thicknesses, and taking account of 1D velocity variations.

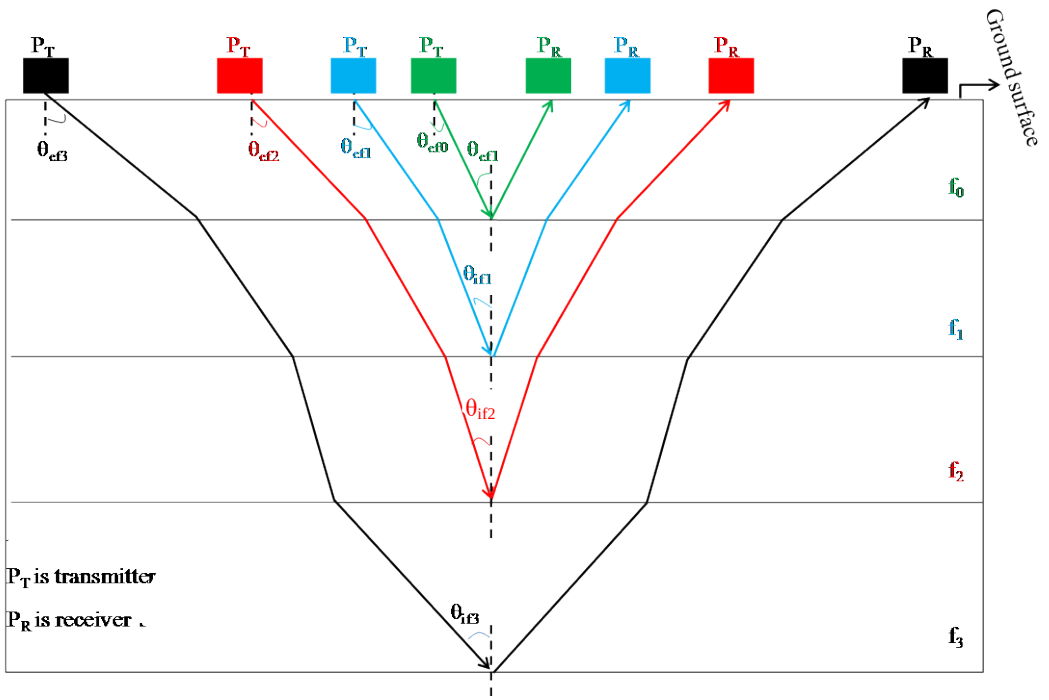

Figure 3: A schematic representation of a CMP geometry showing emergence and incidence angles (i.e. θ_e and θ_i respectively) for successive reflections.

CMP data acquisition and processing

Two transverse electric TE mode CMP data sets (i.e. CMP2a and CMP2b) were collected on the horizontal quarry floor using a 500 MHz Pulse Ekko Pro GPR system by Sensors and Software. The data were processed using the Reflex - Win version 3.5.1 (Sandmeier

1997 - 2004). In order to preserve the amplitude characteristics which the analysis requires, the following processing was done: de-wow, time-zero corrections, band - pass filtering, gain, migration and Hilbert transform. Table 1 summarizes data acquisition parameters.

Table 1: CMP data acquisition parameters

Parameter	Value
Antenna polarity	TE
Maximum/minimum offset (m)	0.24/19.00
Sampling interval (ns)	0.2
Trace increment (m)	0.04
Record length (ns)	400
Stack	64
Centre frequency (MHz)	500

Semblance analysis was done to estimate velocity distribution with depth; interval velocity ranges between 0.087 m/ns and 0.122 m/ns, relative permittivity in these intervals is between 6 ± 0.6 and 11.9 ± 0.1. Figure 3 shows the CMP data sets and semblance windows.

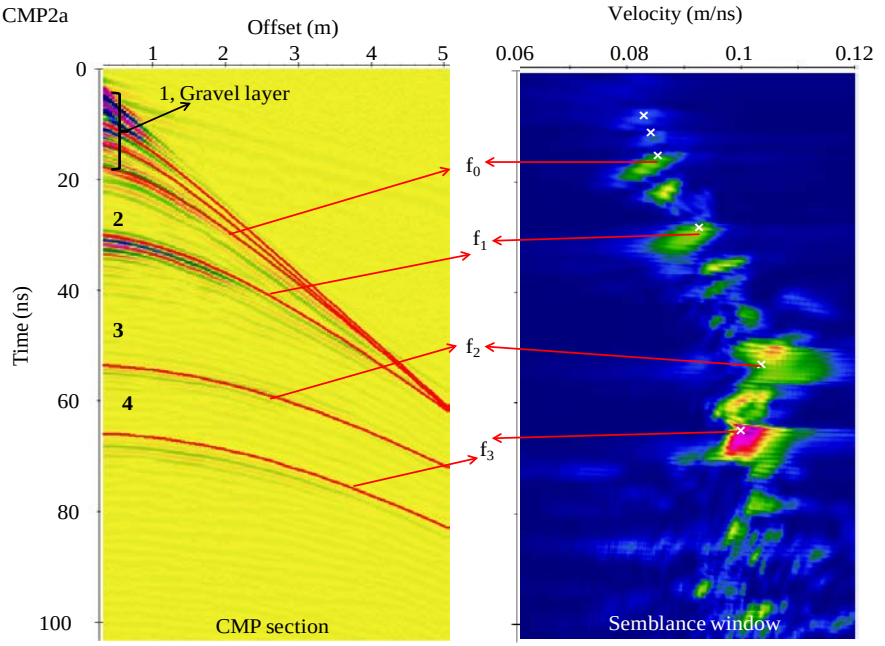

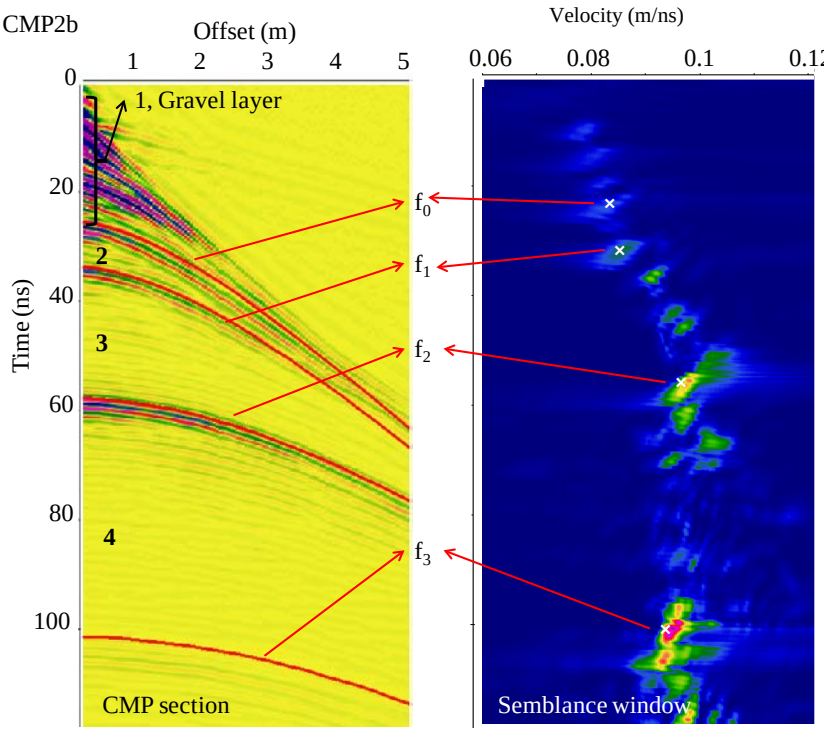

Figure 4: CMP2a and CMP2b data sets along with semblance analysis windows. CMP data show coherent reflections interpreted as bedding plane fractures separating limestone layers. The first layer in each case is a gravel layer

Spectral ratios analysis on the CMP data

In fitting a straight line to the spectral ratios, a bandwidth needs to be selected; to do this, interference - free regions of the amplitude spectra need to be considered. CMP2a and CMP2b sections are interpreted as comprising gravel layer (layer 1) which overlies solid limestone – layers 2, 3 and 4. Layer 1 in these CMP sections cannot be characterized using the spectral ratio method because the method requires comparing two wavelets from the top and bottom surfaces of a layer. It is however expected that attenuation will be relatively high (relative to other layers) due to the presence of fissures which may contain water. Q* was extracted for the underlying solid limestone i.e. layers 2, 3 and 4 in the CMP sections.

The process of extracting Q* (and hence, α) for all layers in all CMP sections is similar: the only difference is in the choice of analysis bandwidth, i.e. range of frequencies to fit a straight line to. As examples, amplitude spectra and corresponding spectral ratios plot for only layer 4 in each CMP section will be shown.

In all cases, I chose a bandwidth to include all relevant frequency content i.e. excluding regions of interference; for example, in layer 4 of CMP2a (figure 5), the bandwidth containing relevant data is between 250 MHz and 900 MHz, I used data between 430 MHz and 860 MHz to avoid interference between 250 MHz and 430 MHz in f_2 spectra (figure 5a).

Figures 6 *a* - *c*, and 8 *a* - *c* show attenuation versus (analysis) frequency for CMP2a and CMP2b layers respectively. For each frequency, α is calculated for all emergence angles, then the average of the resulting values is shown as a function of frequency in these plots.

Attenuation generally increases with frequency which is not surprising since high frequency components are attenuated faster than lower frequencies; the variation in α with emergence angles also increases with frequency.

Figures 6 *d* – *f* and 7*d* - *f* show attenuation values at 500 MHz frequency versus emergence angles, for CMP2a and CMP2b layers respectively. In CMP2a, α (m^{-1}) is highest at an emergence angle of 20° in all layers (figures 6 *d* – *f*) which is in the region of the critical angle (17°) where the maximum radiation into the ground occurs. In CMP2b, the emergence angles analysed are less than the critical angle (18°) in all layers (figures 8 *d* - *f*); attenuation still varies with emergence angle.. The variations in α (m^{-1}) with emergence angle point to the heterogeneous nature of the limestone. This heterogeneity is expected in natural rocks which are not perfectly homogeneous.

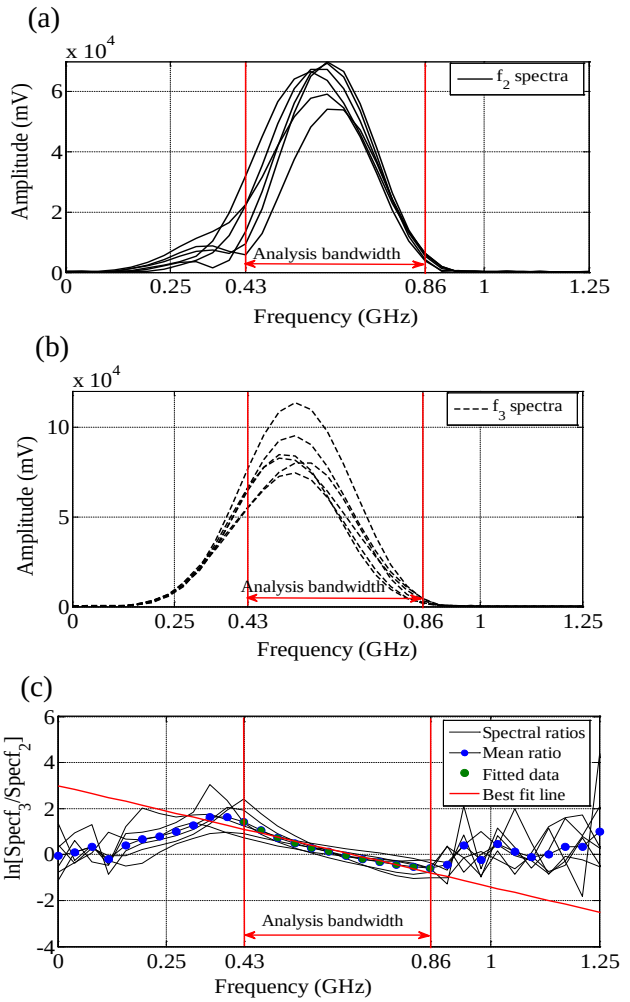

Figure 5: CMP2a (a) f_2 amplitude spectra, (b) f_3 amplitude spectra and (c) spectral ratios between f_3 and f_2 i.e. layer 4. The analysis bandwidth was chosen to include relevant frequency content (0.25 GHz to 0.86 GHz); but because of the interference between 0.25 GHz and 0.43 GHz affecting f_2 spectra, the analysis bandwidth was limited to between 0.43 GHz and 0.86 GHz. The different curves correspond to f_2 and f_3 emergence angles.

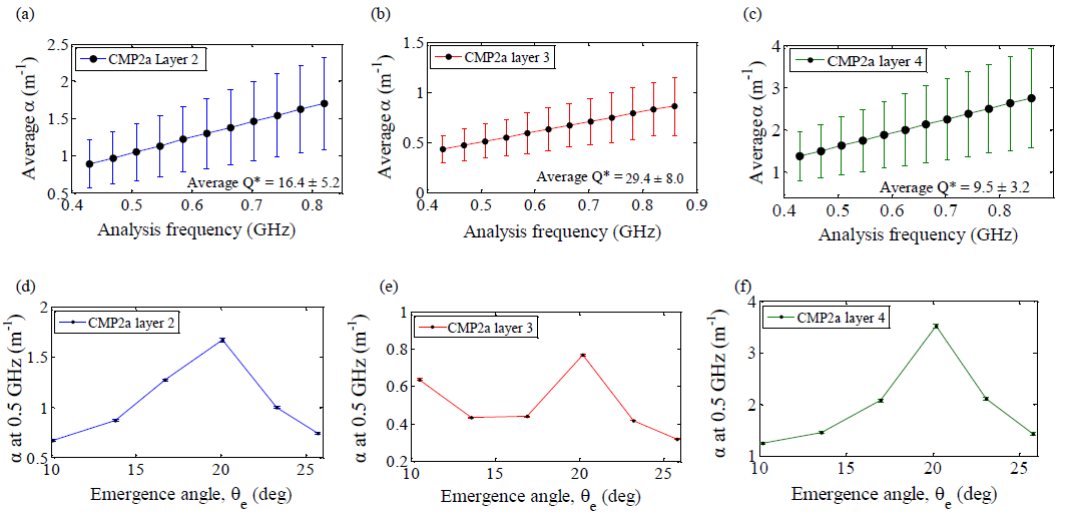

Figure 6: CMP2a Spectral ratios analysis, (a), (b) and (c) average α values (with respect to emergence angles) versus analysis frequency for layers 1 to 3; error bars correspond to 1 standard deviation. (d), (e) and (f) layers 2, 3 and 4 α values at 500 MHz versus (common) emergence angles for compared reflections; error bars are regression derived standard errors propagated using formulas from [10].

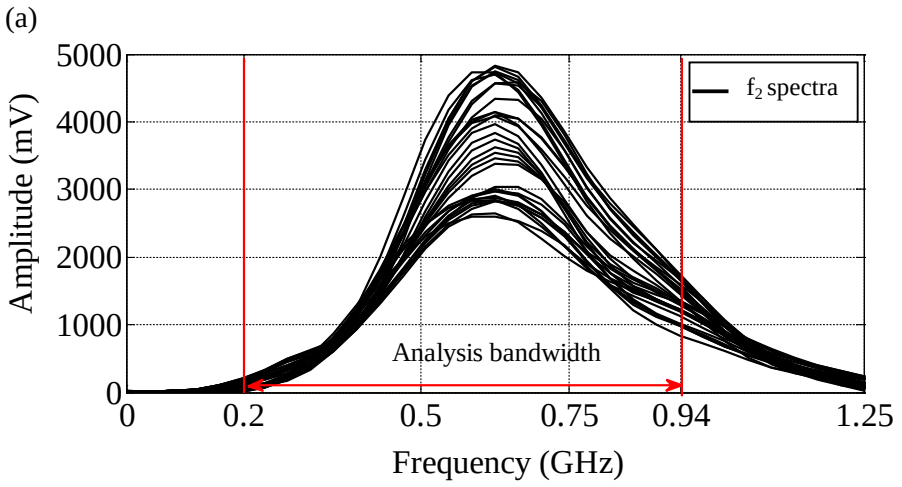

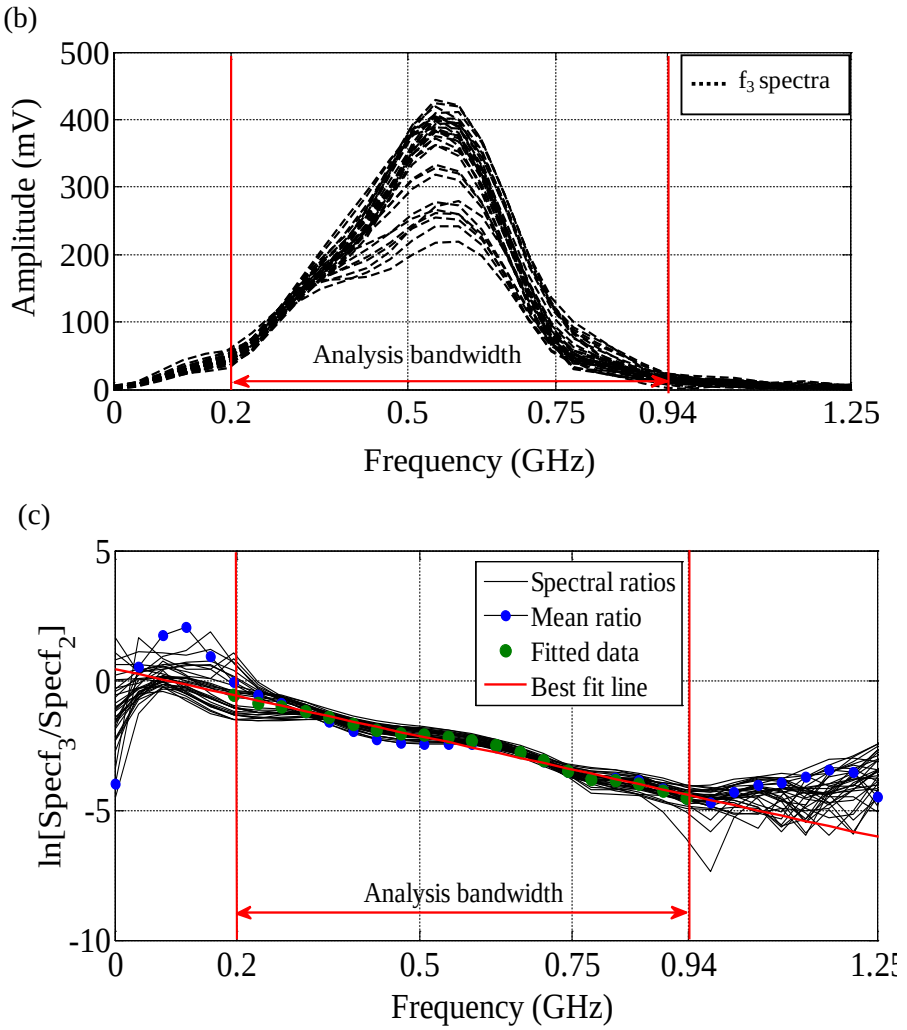

Figure 7: CMP2b (a) f_2 amplitude spectra, (b) f_3 amplitude spectra and (c) spectral ratios between f_3 and f_2 i.e. layer 4. The analysis bandwidth was chosen to include relevant frequency content (0.2 GHz to 0.94 GHz).

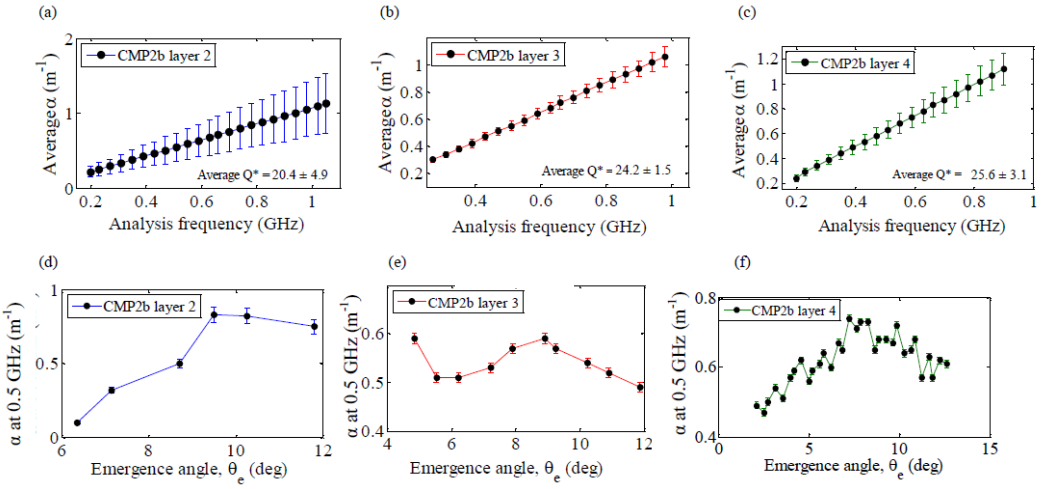

Figure 8: CMP2b Spectral ratios analysis, (a), (b) and (c) average α values (with respect to emergence angles) versus analysis frequency for layers 1 to 3; error bars correspond to 1 standard deviation. (d), (e) and (f) layers 2, 3 and 4 α values at 500 MHz versus (common) emergence angles for compared reflections; error bars are regression derived standard errors propagated using formulas from [10].

Layer 2	
Q*	16.4 ± 5.2
α (m^{-1})	1 ± 0.4
σ (Sm^{-1})	0.2 ± 0.1

Layer 3	
Q*	29.4 ± 8
α (m^{-1})	0.5 ± 0.1
σ (Sm^{-1})	0.09 ± 0.03

Layer 4	
Q*	9.5 ± 3.2
α (m^{-1})	2 ± 0.8
σ (Sm^{-1})	0.4 ± 0.2

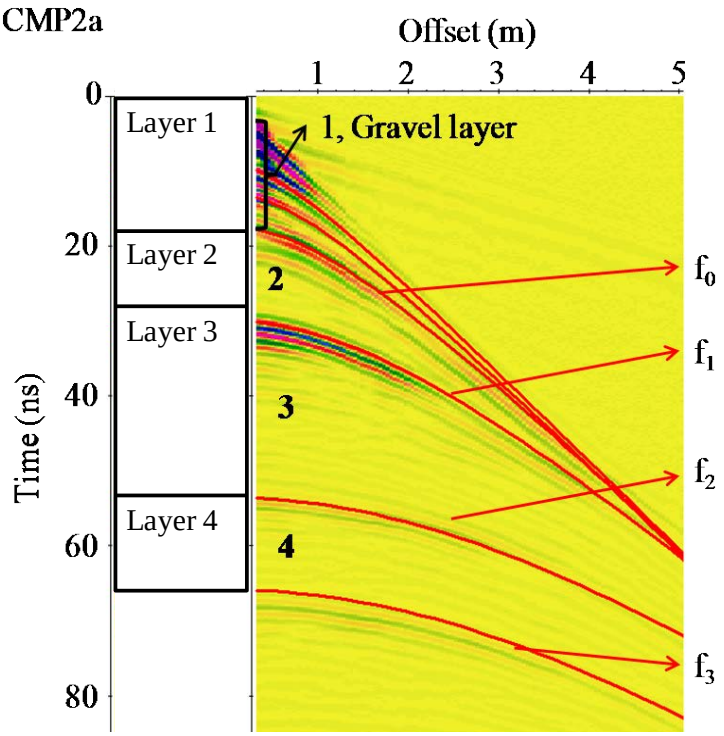

Figure 9: CMP2a section and corresponding attenuation coefficient, α (at 500 MHz), for layers 2, 3 and 4. Attenuation coefficient is expressed in $m^{-1} = 20\log_{10}(\exp^{(\alpha m-1)})$ dBm^{-1}.

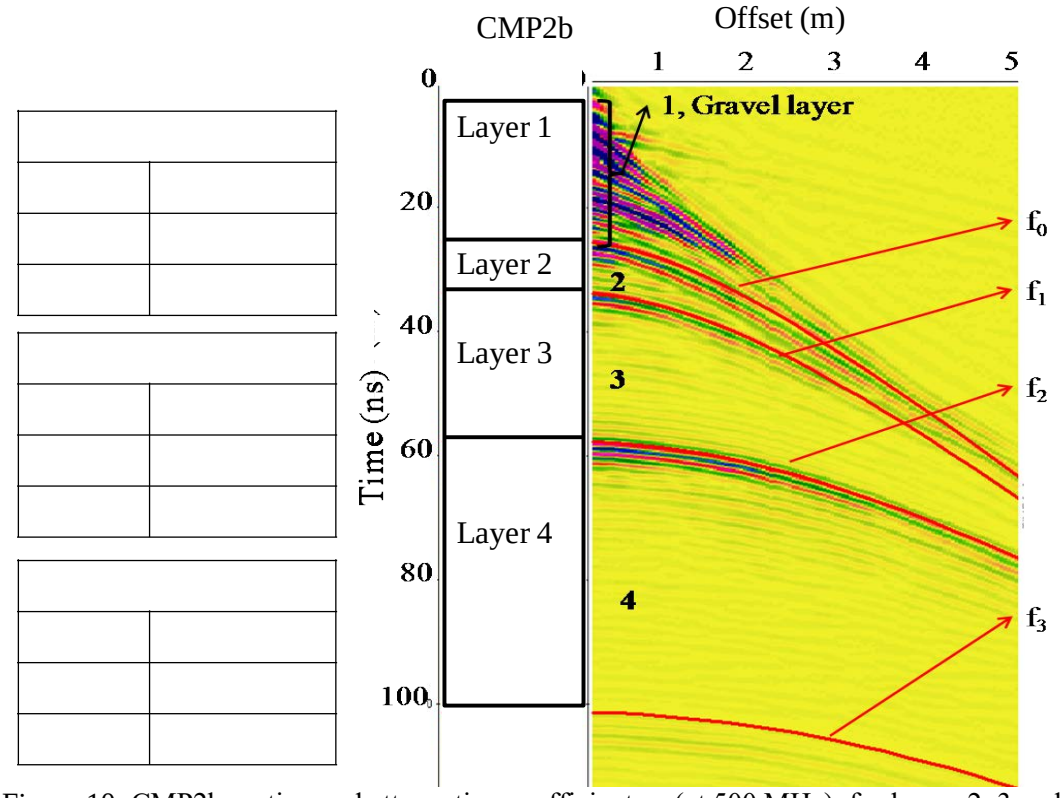

Figure 10: CMP2b section and attenuation coefficients α (at 500 MHz), for layers 2, 3 and 4. Attenuation coefficient is expressed in $m^{-1} = 20\log_{10}(\exp^{(\alpha m-1)})$ dBm^{-1}.

Figures 9 and 10 show average Q*, attenuation (α) and equivalent electrical conductivity (σ) calculated for a frequency of 500 MHz for all layers in the CMP sections; error bars correspond to 1 standard deviation (of attenuation values with emergence angles). Attenuation generally decreases with depth except in CMP2a layer 4 where α is poorly constrained i.e. 2 ± 0.8 m^{-1} (figure 9); layer 4 may contain a significant amount of clay leading to the high attenuation value obtained. The general decrease is due to the limestone being less fractured with depth and therefore decreasing water content. Table 2 compares the attenuation coefficient values obtained here and published values for limestone, it is seen that the values obtained here overlap the range of published values.

Table 2: A comparison between attenuation coefficients obtained here and published values.

Source of attenuation values	α (m^{-1})	α (dBm^{-1})
This paper 100 MHz	0.08 ± 0.01 - 0.19 ± 0.04	0.69 ± 0.09 - 1.7 ± 0.4
Davis and Annan (1989) 100 MHz	0.05 - 0.12	0.4 - 1
This paper 500 MHz	0.4 ± 0.06 - 1.0 ± 0.2	3.5 ± 0.5 – 8.6 ± 3.4
Turner and Siggins (1994) 500 MHz	~0.8	~7

3 Conclusions

Conductive attenuation is of great significance in all analysis of GPR data, it is described by the attenuation coefficient, α which is fractional loss per unit distance (per *m* in this case) of propagation; this was measured using the spectral ratio method, which yields attenuation versus frequency; using this method has the advantage of *in – situ* characterization, because it is done on the CMP data itself which is then further analysed with the AVA method.

References

[1] Aki K., and Richards P. G. Quantitative Seismology: Theory and Methods. Freeman, San Francisco, (1980).

[2] Axtell C., Whittaker J., Clark R. A., Booth A., & Murray T. Measuring GPR attenuation from CMP gathers using common angle and common slowness methods. *17th European Meeting of Environmental and Engineering Geophysics of the Near Surface Geoscience Division of EAGE. Leicester, UK, 12 to 14 September 2011*, (2011).

[3] Dasgupta R., and Clark R. A. Estimation of Q from surface seismic reflection data. *Geophysics*, **63**, (1998) pp 2120 - 2128.

[4] Irving J. D., and Knight R. Removal of wavelet dispersion from ground penetrating radar. *Geophysics*, **68**, (2003), pp 960 - 970.

[5] Powers M. H. Modelling frequency-dependent GPR. *The Leading Edge*, **16**, (1997) pp 15657 - 1662.

[6] Reine C. M., van der Bann., and R. A. Clark. The robustness of seismic attenuation measurements using fixed- and variable-window time frequency transforms. *Geophysics*, **74**, (2), (2009) pp WA123-WA135.

[7] Sears F. M., and Bonner B. P. Ultrasonic attenuation measurements by spectral ratios utilising signal processing techniques. *IEEE transactions on Geoscience and Remote Sensing*, GE **19**, (1981) pp 95 - 99.

[8] Sheriff, R. E. Encyclopedic dictionary of Geophysics. Society of Exploration Geophysicists SEG, (2002).

[9] Tonn R. The determination of the seismic quality factor Q from VSP data: a comparison of different computational methods: *Geophysical Prospecting* , **39**, (1991) pp 1 - 27.

[10] Topping J. Errors of observation and their measurements. Chapman and Hall Science Paperbacks,(1971).

[11] Turner G., and Siggins A. F. Constant Q attenuation of subsurface radar pulses. *Geophysics*, **59**, (1994) pp 1192 - 1200.